Chemistry and Physics of Lipids 221 (2019) 114–119

Contents lists available at ScienceDirect

Chemistry and Physics of Lipids

journal homepage: www.elsevier.com/locate/chemphyslip

Review

Single-particle cryo-EM studies of transmembrane proteins in SMA copolymer nanodiscs

Chang Sun*, Robert B. Gennis

Department of Biochemistry, University of Illinois, 600 S. Mathews Street, Urbana, IL 61801, United States

ARTICLE INFO

Keywords:
Styrene-maleic acid copolymer
SMA
Nanodisc
Membrane protein
Cryo-EM
Alternative complex III
Multidrug transporter AcrB
Lipid-protein interaction
Triacylated cysteine

ABSTRACT

Styrene-maleic acid (SMA) copolymers can extract membrane proteins from native membranes along with lipids as nanodiscs. Preparation with SMA is fast, cost-effective, and captures the native protein-lipid interactions. On the other hand, cryo-EM has become increasingly successful and efficient for structural determinations of membrane proteins, with biochemical sample preparation often the bottleneck. Three recent cryo-EM studies on the efflux transporter AcrB and the alternative complex III: cyt *c* oxidase supercomplex have demonstrated the potential of SMA nanodisc samples to yield high-resolution structure information of membrane proteins.

1. Structural studies of the membrane proteins

Membrane proteins play pivotal roles in energy transduction, the immune response, metabolite/drug transport and signal transduction. Structural studies of such proteins generally require isolating them from the native membrane with detergents before characterization with biophysical techniques. NMR, X-ray crystallography and cryo-EM are especially useful due to their capacity to deliver high-resolution structural information. Particularly, single-particle cryo-EM has received increasing attention because it lifts the prerequisite of difficult crystallization of membrane protein and is suitable for a wide range of protein complexes from 60 kDa up to 2.3 MDa (Murata and Wolf, 2018). Furthermore, cryo-EM uses only a small quantity of protein, making it possible to study membrane proteins that can be obtained only at low yields. Together with developed pipelines of data collection and analysis, cryo-EM is now able to solve membrane protein structure at a rapid pace (Cheng, 2018). During the first quarter of 2018, nearly 40% of the membrane protein structures deposited were solved by cryo-EM (Cheng, 2018).

Despite this remarkable achievement, high-resolution cryo-EM intrinsically relies on stable and homogeneous biochemical preparations, which usually requires laborious screening before the expensive large-scale data collection. One key parameter to be optimized is the membrane-mimetic environment that is utilized, including detergents, bicelles, membrane scaffold protein (MSP) nanodiscs, amphipols, and styrene-maleic acid (SMA) copolymers. In contrast to micelle-forming detergents, SMA is believed to wrap around the membrane protein along with its surrounding lipids, forming disc-shaped structures often referred as SMA lipid particles (SMALPs) or SMA nanodiscs (Dorr et al., 2016). Unlike MSP and amphipols which require the use of detergents during membrane solubilization, SMA has been shown to effectively extract both prokaryotic (Dorr et al., 2014; Knowles et al., 2009; Paulin et al., 2014; Prabudiansyah et al., 2015; Reading et al., 2017; Swainsbury et al., 2014, 2018; Swainsbury et al., 2017) and eukaryotic (Gulati et al., 2014; Jamshad et al., 2015, 2011; Long et al., 2013; Rehan et al., 2017; Skaar et al., 2015; Smirnova et al., 2016) membrane proteins from native membrane, and sometimes confer superior protein stability compared to traditional detergents (Jamshad et al., 2015; Rehan et al., 2017; Swainsbury et al., 2014).

Quite recently, Parmar et al. (2018) and Sun et al. (2018) have reported independently cryo-EM studies with SMALPs which have clearly demonstrated the usefulness of SMA in cryo-EM studies. In this review, we will briefly go through the structural findings enabled by the happy marriage between SMA and electron microscopy, hoping to convince the reader that SMA is an excellent addition to the arsenal for structural studies of membrane proteins.

2. Negative-staining EM of membrane proteins in SMA nanodiscs

Negative-staining EM is a powerful and straight-forward technique

* Corresponding author. Current address: Vollum Institute, Oregon Health & Science University, Portland, OR, 97239, United States.
E-mail address: sun.changing@gmail.com (C. Sun).

https://doi.org/10.1016/j.chemphyslip.2019.03.007
Received 1 December 2018; Received in revised form 14 March 2019; Accepted 14 March 2019
Available online 30 March 2019
0009-3084/ © 2019 Elsevier B.V. All rights reserved.

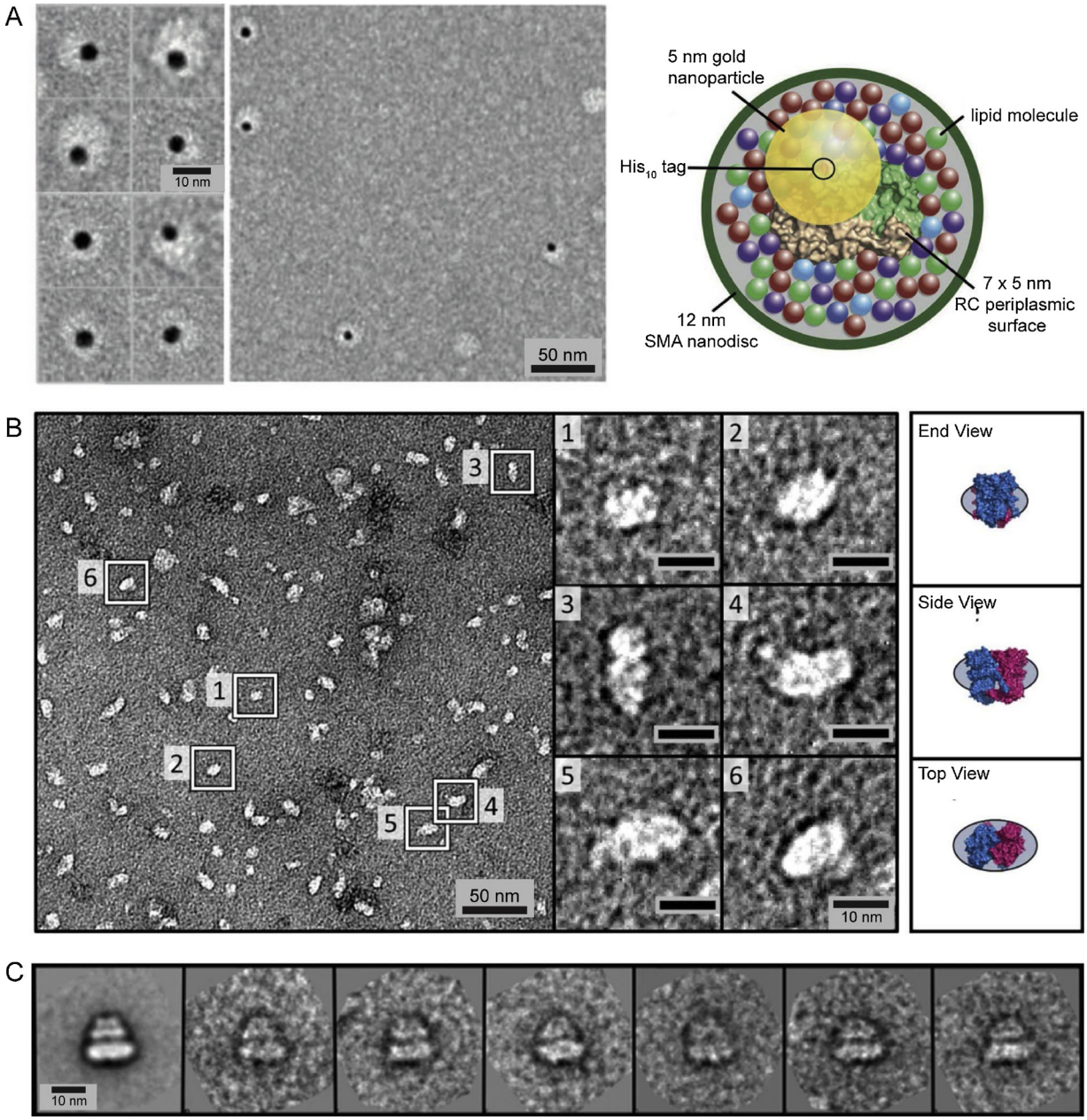

Fig. 1. Negative-staining EM of membrane proteins in SMA nanodiscs. A, Negative-staining EM micrograph and schematic of bacterial reaction center conjugated with 5 nm gold nanoparticles at its 10x histidine tag in SMA nanodiscs (Swainsbury et al., 2014). Notice, there are also unlabeled reaction centers in the micrograph. This panel has been modified with permission from Wiley. B, Negative-staining EM micrograph of the dimeric bc_1 complex in SMA nanodiscs (Swainsbury et al., 2018). This panel has been modified with permission from Elsevier. C. 2D class average and individual particles of AcrB in SMA nanodiscs (Postis et al., 2015). Copyright Postis et. al, licensed under CC-BY.

to visualize biological samples. In 2009, negative-staining EM characterization of palmitoyl transferase PagP in DMPC-containing SMALPs reveals that the protein SMA assembly is dispersed as disc-shaped particles with an average diameter of about 10 nm, leading to the idea that SMA wraps around the membrane protein along with the surrounding lipids (Knowles et al., 2009). Later negative-staining EM studies have confirmed the discoidal nature of SMA-solubilized membrane protein particles (Craig et al., 2016; Dorr et al., 2014; Paulin et al., 2014; Swainsbury et al., 2014; Tanaka et al., 2015). Notably, Swainsbury et al. (2014) conjugated the His-tagged bacterial reaction center in SMA nanodiscs with 5 nm Ni-nitrilotriacetic acid (NTA) functionalized gold nanoparticles, which are distinctive in the negative-staining EM micrographs and serve as a ruler to gauge the size of SMA nanodiscs (Fig. 1A). Though SMA nanodisc samples commonly appear as top views in negative-staining EM, they can also be viewed in other orientations. One such example is the dimeric cyt bc_1 in SMA nanodiscs, where particles corresponding to different views can be picked (Fig. 1B). Intriguingly, in the case of multidrug transporter AcrB, the dominant view of its SMA nanodiscs is the side view (Fig. 1C), from which the transmembrane domain and the periplasmic domain are clearly distinguishable. However, negative-staining EM is inherently limited to a resolution of about 20 Å and doesn't hold promise to obtain finer structural details such as secondary structure and side chain position.

3. Cryo-EM studies of multidrug transporter AcrB

AcrB is a bacterial multidrug efflux transporter that utilizes the

transmembrane proton electrochemical gradient to pump substances, including drug molecules, out of the bacterium. The transporter is a homotrimer with an overall molecular weight of 342 kDa. From previous X-ray crystallography structures, it is known to adopt a jellyfish-shaped architecture with a three-fold symmetry axis perpendicular to the membrane (Murakami et al., 2002). As is shown in Fig. 1C, the characteristic shape of AcrB can be resolved at the single-particle level using negative-staining EM.

AcrB with a C-terminal 8xHis tag is over-expressed in the C43(DE3) *E. coli* strain and extracted from the membrane with 2:1 SMA copolymer. A 3 μL-drop of purified AcrB in SMA nanodiscs (1 mg/mL) is applied onto a glow-discharged gold grid and blotted with ash-free filter paper using the Vitrobot Mark IV before freezing in liquid ethane. Cryo-EM Data are collected at the Astbury Biostructure facility on a G2 Titan Krios equipped with a Falcon III direct electron detector.

The 3D reconstruction of AcrB shows a transmembrane domain and a protruding dome-like structure, where it is expected to interact with the outer membrane channel TolC. The enlargement of the transmembrane domain compared with the crystal structure is consistent with SMA copolymer/ lipids surrounding the protein trimer. From the local resolution analysis (Fig. 2A), it is clear that the periplasmic domain is better resolved at around 7–8 Å. At this resolution, de novo model-building is not possible but flexible fitting of existing structure can be used to obtain the molecular interpretation of the EM density map. Fitting of the crystal structure of AcrB into the density map shows no significant difference (Fig. 2B). The periplasmic domain follows the cryo-EM density closely while part of the transmembrane helices is not accounted for by the density (Fig. 2C). It has been reasoned that the SMA copolymer may interact with the protein transmembrane helices and increase their mobility (Parmar et al., 2018).

During the peer reviewing of this manuscript, another cryo-EM study of AcrB in 2:1 SMA nanodiscs was published with a much-improved resolution of 3.2 Å (Qiu et al., 2018). At this resolution, the interpretability of the density map is extended to the level of individual residual, which is evident from the “pitches” of the transmembrane helices (Fig. 3A). Remarkably, there is a bilayer patch of 24 native lipid molecules trapped in the center of the AcrB trimer (Fig. 3B), which is lost in crystal structures after detergent solubilization. The bilayer patch is suggested to supports and harmonizes peristaltic motions through AcrB trimers during its transport cycle. Additionally, there are also a few annular lipids identified in this structure (Fig. 3B).

4. Cryo-EM studies of alternative complex III: cyt *c* oxidase supercomplex

Alternative complex III (ACIII) is a quinol: cyt *c* oxidoreductase found in some bacteria. Based on sequence analysis and biochemical studies, the proposed working model is drastically different from its functional counterpart–bc_1 complex (Refojo et al., 2010a). Additionally, ACIII from *Rhodothermus marinus* has been reported to associate with cyt *c* oxidase and form a functional supercomplex (Refojo et al., 2010b).

To elucidate the molecular mechanism of the ACIII and the configuration of the supercomplex, Sun et al. carry out a cryo-EM study with protein samples prepared in SMA nanodiscs (Sun et al., 2018). Both the ACIII and the cyt *c* oxidase are natively expressed without any genetic modification. After the solubilization with 3:1 SMA copolymer, functional supercomplex is purified taking advantage of the innate affinity of cyt *c* oxidase towards Ni-NTA resin. A 3 μL-drop of sample (3 mg/ml) is applied to gold-coated holey carbon grids and blotted with a FEI Vitrobot before freezing in a 1:1 (v:v) liquid ethane/propane mixture. Cryo-EM data are then collected in the New York Structural Biology Center with a FEI Titan Krios electron microscope equipped with a Gatan K2 Summit camera.

The 3D reconstruction of the supercomplex has a global resolution of 3.6 Å and is readily segmented into the two component protein complexes (Fig. 4A). Local resolution analysis reveals that the ACIII component of the supercomplex is better resolved than the cyt *c* oxidase component. However, unlike the AcrB structure, there is no difference in resolution between the periplasmic domain and the transmembrane domain of ACIII (Fig. 4B). Because all the secondary structure elements are recognizable at this resolution, different subunits of the ACIII are identified and modelled de novo, including all the metal cofactors involved in electron transfer (Fig. 5). This structure of ACIII in SMA is consistent with the proposed enzymatic mechanism for its quinol: cyt *c* activity and rules out the Q-cycle mechanism for ACIII. The structure obtained in SMA nanodiscs shares the same protein architecture as the structure of the *R. marinus* ACIII obtained in detergent (n-Dodecyl β-D-maltoside) from a concurrent, independent study (Sousa et al., 2018).

Eleven phospholipid molecules are resolved in the structure, in addition to two covalent lipids predicted from lipobox sequence motifs present in both the ActB and ActE subunits (Fig. 6). Only the portion of the cyt *c* oxidase component of the supercomplex that is near the interface of ACIII is well resolved, but a complete model of supercomplex

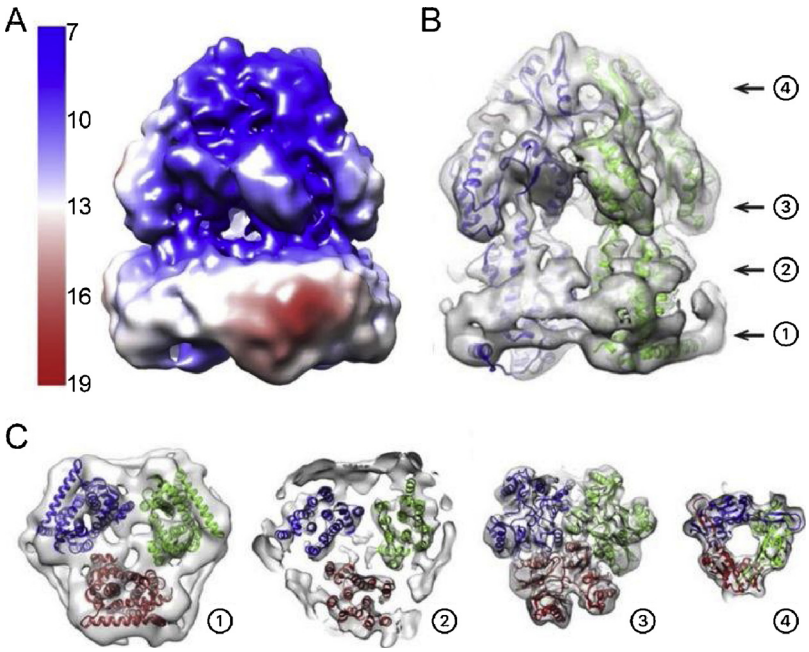

Fig. 2. Cryo-EM of the bacterial multidrug exporter AcrB in SMA nanodiscs. A, 3D reconstruction of the AcrB with its surface colored by local resolution in angstrom. B, Overall fitting of the crystal structure of AcrB in the cryo-EM density map. Arrows and symbols indicate the positions which correspond to section views in panel C. C, Section views of the fitting of the crystal structure of AcrB in the cryo-EM density map. All three panels have been modified from (Parmar et al., 2018). Copyright Parmar et. al., licensed under CC-BY.

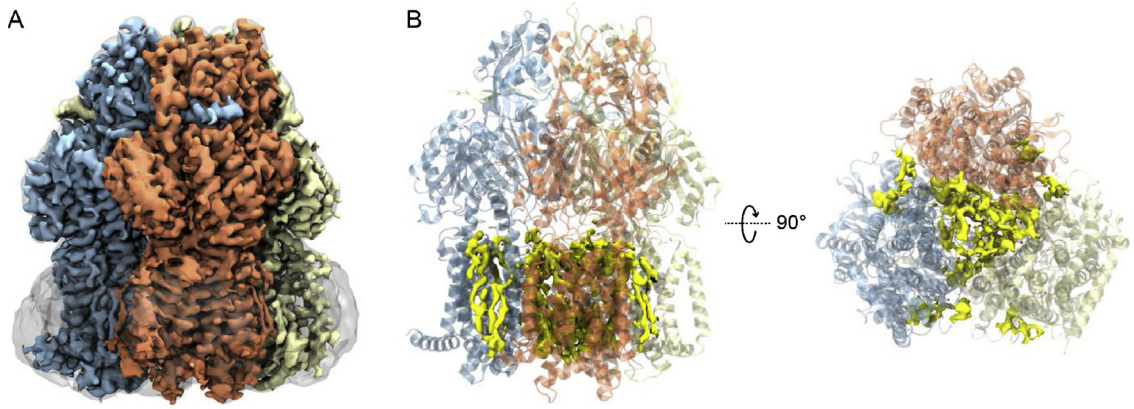

Fig. 3. More recent cryo-EM studies on AcrB in SMA nanodiscs. A, 3D reconstruction of the AcrB. Each protomer of the AcrB trimer are colored differently. Also shown is a smoothed transparent surface of the SMA nanodisc at a lower density value. B, Cartoon representation of the AcrB structure with superimposed EM density of lipids (yellow) in both the central cavity and the annular sites. Both panels are prepared with vmd (Humphrey et al., 1996) using density map and coordinates from entry EMDB-7074 of the Electron Microscopy Data Bank.

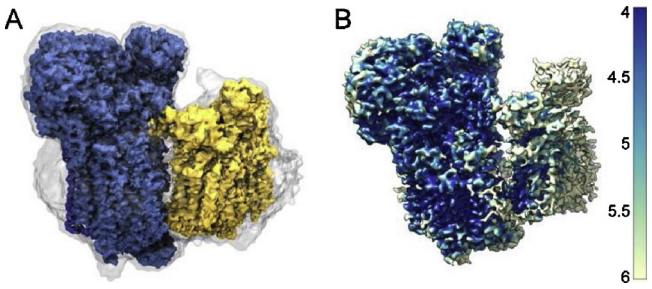

Fig. 4. Cryo-EM of the alternative complex III: cyt *c* oxidase supercomplex in SMA nanodiscs. A, 3D reconstruction of the supercomplex. The ACIII is colored in blue while the cyt *c* oxidase is colored in yellow. Also shown is a smoothed transparent surface of the SMA nanodisc at a lower density value. This panel has been reproduced with permission from Springer Nature. B, 3D reconstruction of the supercomplex colored by local resolution in angstrom.

can be assembled from the cryoEM data by using the existing X-ray structure of related cyt *c* oxidases. Only subunit III of cyt *c* oxidase interacts with ACIII, forming a wedge-like space between the membrane domains of ACIII and complex IV (Sun et al., 2018). In sharp contrast, the cyt *bcc* (complex III) and cyt aa_3 (complex IV) from *Mycobacterium smegmatis* are held together by both lipid-mediated interactions and extensive protein-protein interactions, resulting in a permanent electron transfer pathway from complex III to complex IV (Gong et al., 2018). Nevertheless, the configuration of ACIII: cyt *c* oxidase supercomplex is compatible with an efficient electron-channeling mechanism involving the tethered water-soluble cyt *c* from ActA as the electron carrier.

5. Discussion and conclusion

The most commonly used SMA polymers are industrial low-molecular-weight random copolymers (from Cray Valley and Polyscope) with an overall molar ratio of 2:1 or 3:1 between styrene and maleic acid moieties. These polymers are cost-effective and can extract membrane proteins from native membrane along with lipids as nanodiscs, which can generally stabilize the maintain the function of membrane proteins.

Just as other membrane-mimetic environments, the SMA copolymer has its own limitations. SMA is not a universal solution for the extraction and characterization of all membrane proteins. The efficiency of protein extraction from the native membrane varies and needs to be optimized. Also, SMA may inhibit the function of some membrane enzymes as demonstrated with 3:1 SMA and cytochrome *c* oxidase from *Saccharomyces cerevisiae* (Smirnova et al., 2016). It is important to perform functional assays SMA copolymers with any new protein prior to the cryo-EM studies. At this point, commercially available 2:1 and 3:1 SMA products are random copolymers with heterogeneity in polymer length and monomer sequence distribution, which might lead to a batch-to-batch variation in their membrane solubilizing properties. In addition, the SMA copolymer is only soluble at pH above 7 and

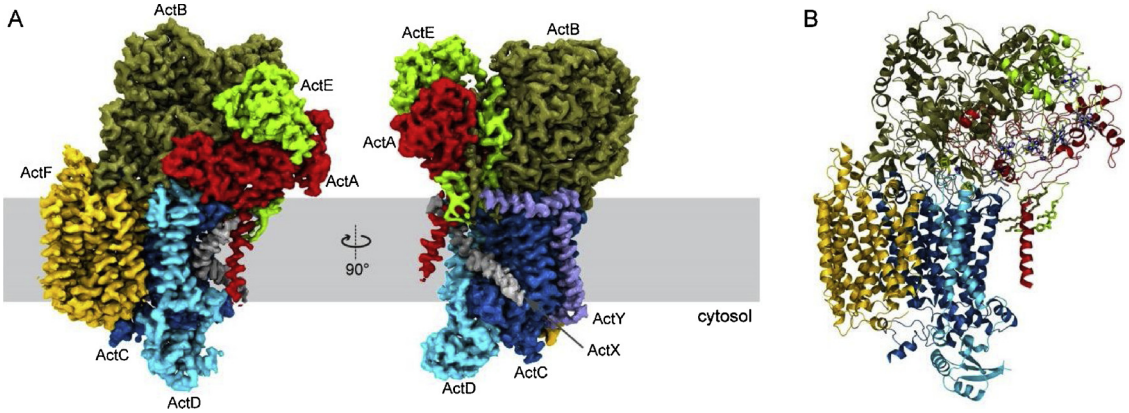

Fig. 5. Structure of the alternative complex III. A, 3D reconstruction of the ACIII colored by subunit. In addition to the six known subunits (ActA to ActF) from the ACIII operon, two small transmembrane peptides ActX and ActY are observed. B, Cartoon representation of the de novo structure of the ACIII colored by subunit. ActX and ActY are not included. Both panels have been modified with permission from Springer Nature.

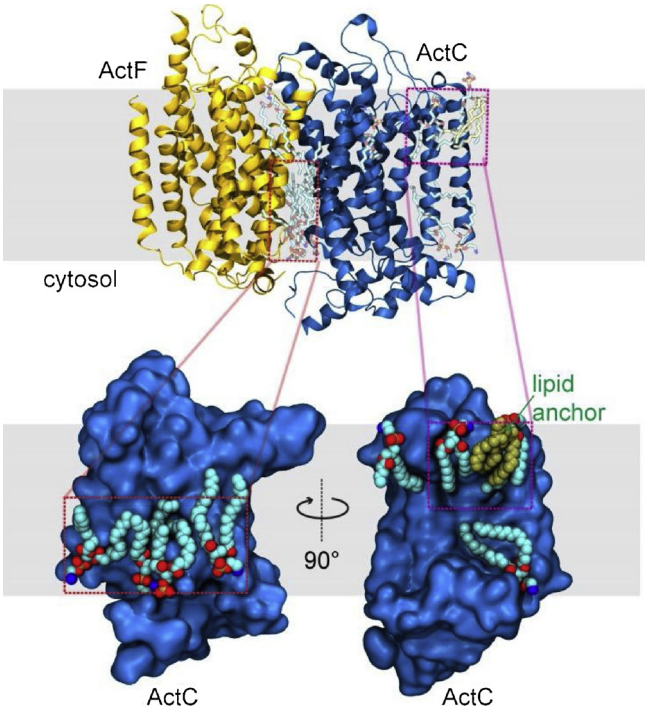

Fig. 6. Lipids resolved in the cryo-EM ACIII structure. Four lipid molecules are resolved at the cytoplasmic interface between ActC and ActF. Besides, two lipid molecules clustered near the triacylated cysteine from ActB, right above the proposed menaquinone entry pathway. This figure has been reproduced with permission from Springer Nature.

cannot tolerate the presence of divalent cations at mM concentrations (Dorr et al., 2016). In response to these issues, SMA copolymers have been synthesized through RAFT polymerization resulting better-defined composition (Craig et al., 2016; Smith et al., 2017), and various derivatives have been reported which offer improved compatibility with buffer pH and divalent cations (Fiori et al., 2017; Ravula et al., 2018, 2017). These advances have expanded the range of conditions where SMA can be applied to yield nanodiscs.

As is demonstrated by the three recent cryo-EM studies summarized here, SMA nanodisc samples are compatible with cryo-EM and these preparations can yield high-resolution structural information. This approach is well-suited to study the lipid-protein interactions under physiological conditions since native lipids are co-extracted with the proteins. Although both of the structural studies discussed here are on prokaryotic membrane proteins, SMA nanodiscs containing eukaryotic proteins should be equally amenable to cryo-EM studies. We are confident that more cryo-EM membrane protein structures will be solved in the SMA copolymer nanodiscs.

Conflict of interest statement

Nothing to declare.

Acknowledgement

This work is funded by NIH Grant HL16101 (to R.B.G.).

References

Cheng, Y., 2018. Membrane protein structural biology in the era of single particle cryo-EM. Curr. Opin. Struct. Biol. 52, 58–63.
Craig, A.F., Clark, E.E., Sahu, I.D., Zhang, R., Frantz, N.D., Al-Abdul-Wahid, M.S., Dabney-Smith, C., Konkolewicz, D., Lorigan, G.A., 2016. Tuning the size of styrene-maleic acid copolymer-lipid nanoparticles (SMALPs) using RAFT polymerization for biophysical studies. Biochim. Biophys. Acta 1858, 2931–2939.
Dorr, J.M., Koorengevel, M.C., Schafer, M., Prokofyev, A.V., Scheidelaar, S., van der Cruijsen, E.A., Dafforn, T.R., Baldus, M., Killian, J.A., 2014. Detergent-free isolation, characterization, and functional reconstitution of a tetrameric K+ channel: the power of native nanodiscs. Proc. Natl. Acad. Sci. U. S. A. 111, 18607–18612.
Dorr, J.M., Scheidelaar, S., Koorengevel, M.C., Dominguez, J.J., Schafer, M., van Walree, C.A., Killian, J.A., 2016. The styrene-maleic acid copolymer: a versatile tool in membrane research. Eur. Biophys. J. 45, 3–21.
Fiori, M.C., Jiang, Y., Altenberg, G.A., Liang, H., 2017. Polymer-encased nanodiscs with improved buffer compatibility. Sci. Rep. 7, 7432.
Gong, H., Li, J., Xu, A., Tang, Y., Ji, W., Gao, R., Wang, S., Yu, L., Tian, C., Li, J., Yen, H.Y., Man Lam, S., Shui, G., Yang, X., Sun, Y., Li, X., Jia, M., Yang, C., Jiang, B., Lou, Z., Robinson, C.V., Wong, L.L., Guddat, L.W., Sun, F., Wang, Q., Rao, Z., 2018. An electron transfer path connects subunits of a mycobacterial respiratory supercomplex. Science 362, eaat8923.
Gulati, S., Jamshad, M., Knowles, T.J., Morrison, K.A., Downing, R., Cant, N., Collins, R., Koenderink, J.B., Ford, R.C., Overduin, M., Kerr, I.D., Dafforn, T.R., Rothnie, A.J., 2014. Detergent-free purification of ABC (ATP-binding-cassette) transporters. Biochem. J. 461, 269–278.
Humphrey, W., Dalke, A., Schulten, K., 1996. VMD: visual molecular dynamics. J. Mol. Graph. 14, 33–38.
Jamshad, M., Lin, Y.P., Knowles, T.J., Parslow, R.A., Harris, C., Wheatley, M., Poyner, D.R., Bill, R.M., Thomas, O.R., Overduin, M., Dafforn, T.R., 2011. Surfactant-free purification of membrane proteins with intact native membrane environment. Biochem. Soc. Trans. 39, 813–818.
Jamshad, M., Charlton, J., Lin, Y.P., Routledge, S.J., Bawa, Z., Knowles, T.J., Overduin, M., Dekker, N., Dafforn, T.R., Bill, R.M., Poyner, D.R., Wheatley, M., 2015. G-protein coupled receptor solubilization and purification for biophysical analysis and functional studies, in the total absence of detergent. Biosci. Rep. 35.
Knowles, T.J., Finka, R., Smith, C., Lin, Y.P., Dafforn, T., Overduin, M., 2009. Membrane proteins solubilized intact in lipid containing nanoparticles bounded by styrene maleic acid copolymer. J. Am. Chem. Soc. 131, 7484–7485.
Long, A.R., O'Brien, C.C., Malhotra, K., Schwall, C.T., Albert, A.D., Watts, A., Alder, N.N., 2013. A detergent-free strategy for the reconstitution of active enzyme complexes from native biological membranes into nanoscale discs. BMC Biotechnol. 13, 41.
Murakami, S., Nakashima, R., Yamashita, E., Yamaguchi, A., 2002. Crystal structure of bacterial multidrug efflux transporter AcrB. Nature 419, 587–593.
Murata, K., Wolf, M., 2018. Cryo-electron microscopy for structural analysis of dynamic biological macromolecules. Biochim. Biophys. Acta Gen. Sub. 1862, 324–334.
Parmar, M., Rawson, S., Scarff, C.A., Goldman, A., Dafforn, T.R., Muench, S.P., Postis, V.L.G., 2018. Using a SMALP platform to determine a sub-nm single particle cryo-EM membrane protein structure. Biochim. Biophys. Acta 1860, 378–383.
Paulin, S., Jamshad, M., Dafforn, T.R., Garcia-Lara, J., Foster, S.J., Galley, N.F., Roper, D.I., Rosado, H., Taylor, P.W., 2014. Surfactant-free purification of membrane protein complexes from bacteria: application to the staphylococcal penicillin-binding protein complex PBP2/PBP2a. Nanotechnology 25, 285101.
Postis, V., Rawson, S., Mitchell, J.K., Lee, S.C., Parslow, R.A., Dafforn, T.R., Baldwin, S.A., Muench, S.P., 2015. The use of SMALPs as a novel membrane protein scaffold for structure study by negative stain electron microscopy. Biochim. Biophys. Acta 1848, 496–501.
Prabudiansyah, I., Kusters, I., Caforio, A., Driessen, A.J., 2015. Characterization of the annular lipid shell of the Sec translocon. Biochim. Biophys. Acta 1848, 2050–2056.
Qiu, W., Fu, Z., Xu, G.G., Grassucci, R.A., Zhang, Y., Frank, J., Hendrickson, W.A., Guo, Y., 2018. Structure and activity of lipid bilayer within a membrane-protein transporter. Proc. Natl. Acad. Sci. U. S. A. 115, 12985–12990.
Ravula, T., Hardin, N.Z., Ramadugu, S.K., Ramamoorthy, A., 2017. pH tunable and divalent metal ion tolerant polymer lipid nanodiscs. Langmuir 33, 10655–10662.
Ravula, T., Hardin, N.Z., Ramadugu, S.K., Cox, S.J., Ramamoorthy, A., 2018. Formation of pH-Resistant monodispersed polymer-lipid nanodiscs. Angew. Chem. Int. Ed. Engl. 57, 1342–1345.
Reading, E., Hall, Z., Martens, C., Haghighi, T., Findlay, H., Ahdash, Z., Politis, A., Booth, P.J., 2017. Interrogating membrane protein conformational dynamics within native lipid compositions. Angew. Chem. Int. Ed. Engl. 56, 15654–15657.
Refojo, P.N., Sousa, F.L., Teixeira, M., Pereira, M.M., 2010a. The alternative complex III: a different architecture using known building modules. Biochim. Biophys. Acta 1797, 1869–1876.
Refojo, P.N., Teixeira, M., Pereira, M.M., 2010b. The alternative complex III of Rhodothermus marinus and its structural and functional association with caa3 oxygen reductase. Biochim. Biophys. Acta 1797, 1477–1482.
Rehan, S., Paavilainen, V.O., Jaakola, V.P., 2017. Functional reconstitution of human equilibrative nucleoside transporter-1 into styrene maleic acid co-polymer lipid particles. Biochim. Biophys. Acta 1859, 1059–1065.
Skaar, K., Korza, H.J., Tarry, M., Sekyrova, P., Hogbom, M., 2015. Expression and subcellular distribution of GFP-Tagged human tetraspanin proteins in Saccharomyces cerevisiae. PLoS One 10, e0134041.
Smirnova, I.A., Sjostrand, D., Li, F., Bjorck, M., Schafer, J., Ostbye, H., Hogbom, M., von Ballmoos, C., Lander, G.C., Adelroth, P., Brzezinski, P., 2016. Isolation of yeast complex IV in native lipid nanodiscs. Biochim. Biophys. Acta 1858, 2984–2992.
Smith, A.A.A., Autzen, H.E., Laursen, T., Wu, V., Yen, M., Hall, A., Hansen, S.D., Cheng, Y., Xu, T., 2017. Controlling styrene maleic acid lipid particles through RAFT. Biomacromolecules 18, 3706–3713.
Sousa, J.S., Calisto, F., Langer, J.D., Mills, D.J., Refojo, P.N., Teixeira, M., Kuhlbrandt, W., Vonck, J., Pereira, M.M., 2018. Structural basis for energy transduction by respiratory alternative complex III. Nat. Commun. 9, 1728.
Sun, C., Benlekbir, S., Venkatakrishnan, P., Wang, Y., Hong, S., Hosler, J., Tajkhorshid, E., Rubinstein, J.L., Gennis, R.B., 2018. Structure of the alternative complex III in a supercomplex with cytochrome oxidase. Nature 557, 123–126.

Swainsbury, D.J., Scheidelaar, S., van Grondelle, R., Killian, J.A., Jones, M.R., 2014. Bacterial reaction centers purified with styrene maleic acid copolymer retain native membrane functional properties and display enhanced stability. Angew. Chem. Int. Ed. Engl. 53, 11803–11807.

Swainsbury, D.J.K., Scheidelaar, S., Foster, N., van Grondelle, R., Killian, J.A., Jones, M.R., 2017. The effectiveness of styrene-maleic acid (SMA) copolymers for solubilisation of integral membrane proteins from SMA-accessible and SMA-resistant membranes. Biochim. Biophys. Acta Biomembr. 1859, 2133–2143.

Swainsbury, D.J.K., Proctor, M.S., Hitchcock, A., Cartron, M.L., Qian, P., Martin, E.C., Jackson, P.J., Madsen, J., Armes, S.P., Hunter, C.N., 2018. Probing the local lipid environment of the Rhodobacter sphaeroides cytochrome bc1 and Synechocystis sp. PCC 6803 cytochrome b6f complexes with styrene maleic acid. Biochim. Biophys. Acta 1859, 215–225.

Tanaka, M., Hosotani, A., Tachibana, Y., Nakano, M., Iwasaki, K., Kawakami, T., Mukai, T., 2015. Preparation and characterization of reconstituted lipid-synthetic polymer discoidal particles. Langmuir 31, 12719–12726.